ChemComm

COMMUNICATION

View Article Online
View Journal | View Issue

Cite this: *Chem. Commun.*, 2014, 50, 9509

Received 25th March 2014,
Accepted 2nd June 2014

DOI: 10.1039/c4cc02217c

www.rsc.org/chemcomm

Enhanced photoelectric performance of PbS/CdS quantum dot co-sensitized solar cells *via* hydrogenated TiO_2 nanorod arrays†

Yanli Chen,[a] Qiang Tao,[a] Wuyou Fu,[a] Haibin Yang,*[a] Xiaoming Zhou,[a] Shi Su,[a] Dong Ding,[a] Yannan Mu,[ab] Xue Li[a] and Minghui Li[a]

The enhanced photoelectric performance of quantum dot sensitized solar cells *via* hydrogenated TiO_2 is proposed. The best energy conversion efficiency is 1.5 times higher than cells without hydrogen treatment. We demonstrated that introducing oxygen vacancies by hydrogenation is an effective and feasible method for enhanced photoelectric performance.

Titanium dioxide (TiO_2) has been extensively investigated as a photoanode for quantum dot sensitized solar cells (QDSSCs) because of its favorable band-edge positions, strong optical absorption, superior chemical stability, photocorrosion resistance, and low cost.[1] However, its large band gap (~3.2 eV) means that TiO_2 can only harvest UV light, which is just 5% of sunlight, resulting in low energy conversion efficiency. Much effort has been made to improve its visible light harvesting ability. Typically, the methods can be summarized into two categories: one way is narrowing the band gap by doping with metal or nonmetal impurities that generate donor or acceptor states in the band gap,[2] and annealing under a reducing gas atmosphere introducing defect states within the forbidden band can also narrow the band gap.[3] Another strategy that is widely employed in QDSSCs, is sensitizing TiO_2 with multiple narrow band gap semiconductors such as CdS,[4] CdSe,[5] and PbS.[6] In fact, the purpose of these methods is to increase the electrical conduction in the structure, which can fundamentally change the electronic structure of TiO_2, or effectively separate and transport photoexcited charge carriers.

Recently, using hydrogenated TiO_2 (H-TiO_2) to increase the amount of oxygen vacancies has been widely studied in the field of photoelectrochemical water splitting and photocatalysis, achieving excellent results.[7] These excellent results are due to fact that oxygen vacancies on the surface of TiO_2 can enhance photocatalytic activity through charge carrier trapping and prevention of recombination. On the other hand, hydrogen can move rapidly around and yield electronic structure changes from the alteration of orbital overlap in TiO_2. To our knowledge, there has been no systematic research concerning the use of H-TiO_2 in QDSSCs. In order to find out the influence of the oxygen vacancies generated by H-TiO_2 on photoelectric performance, we studied the change in photoelectric performance of TiO_2 nanorod arrays before and after hydrogenation. Besides, to further increase the photoelectric performance, the co-sensitization of TiO_2/H-TiO_2 with PbS/CdS was studied. The results showed that H-TiO_2 can increase the amount of oxygen vacancies, add to the donor density of TiO_2, and improve the photoactivity of TiO_2. It can also gradually narrow the band gap by increasing the hydrogenation temperature, and eventually improve the energy conversion efficiency. We confirmed that the oxygen vacancies generated by hydrogenation can contribute to the improvement of the energy conversion efficiency. Oxygen vacancies generated by hydrogenation will be of great significance in the field of QDSSCs.

TiO_2 nanorod arrays on transparent conductive fluorine-doped tin oxide (FTO) were synthesized by a hydrothermal growth method according to the literature (experimental section, ESI†).[8] The as-prepared TiO_2 nanorod arrays were annealed in air at 550 °C for 3 h, followed by annealing in a hydrogen atmosphere for 30 min at various temperatures in the range of 250–500 °C. As shown the inset of Fig. 1, the color of the H-TiO_2 nanorod array film depends on the hydrogen annealing temperature, it changes from white to black. This indicates that the TiO_2 nanorod arrays show an absorbing ability both in visible light and near-infrared, and also means that the hydrogenation narrowed band gap of TiO_2 is consistent with the results of the diffuse reflectance absorption spectra (Fig. S3(a), ESI†). The black color is ascribed to surface oxygen vacancies of the TiO_2 nanorod arrays.[9]

To determine the crystal structures and possible phase changes during the hydrogenation process, X-ray diffraction (XRD) spectra were collected from the pristine TiO_2 nanorod arrays and H-TiO_2 nanorod arrays prepared at various annealing temperatures, as shown in Fig. 1. After subtracting the diffraction

[a] *State Key Laboratory of Superhard Materials, Jilin University, Changchun 130012, P. R. China. E-mail: yanghb@jlu.edu.cn*

[b] *Department of Physics and Chemistry, Heihe University, Heihe 164300, P. R. China*

† Electronic supplementary information (ESI) available: Detailed synthesis, experimental methods, and additional material characterization. See DOI: 10.1039/c4cc02217c

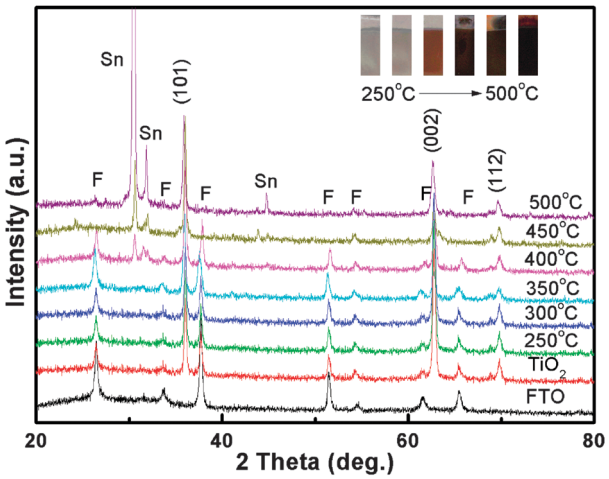

Fig. 1 XRD spectra of pristine TiO_2 and H-TiO_2 nanorod arrays annealed in a hydrogen atmosphere at various temperatures (250, 300, 350, 400, 450, and 500 °C).

peaks of the FTO substrate, three diffraction peaks were observed in every sample at 2θ angles of 36.5°, 63.2° and 69.9° corresponding to the (101), (002) and (112) planes in TiO_2. These sharp peaks are indexed to the characteristic peaks of tetragonal rutile TiO_2 (JCPDS no. 21-1276). Compared to the classical powder diffraction pattern, the (002) diffraction peak at a 2θ angle of 63.2° has the highest intensity. This indicates that the TiO_2 nanorod arrays are highly oriented in the [001] direction on the FTO substrate, which is consistent with the observed growth axis of TiO_2 nanorod arrays (Fig. S1, ESI†). As shown in Fig. 1, there are no phase changes after hydrogenation, although the TiO_2 peak intensity decreases with increasing annealing temperature. This may be due to the increase of the amount of oxygen vacancies in the TiO_2 structure. In addition, the diffraction peaks of the FTO gradually weakened and disappeared, and a group of new peaks were observed corresponding to Sn metal when the annealing temperature was higher than 400 °C. It indicates that the hydrogen treatment at high temperature damaged the FTO conducting layer by decomposing SnO_2 into Sn metal. So we chose an annealing temperature in the hydrogen atmosphere of below 400 °C for our photoelectrodes.

According to our XRD results, hydrogenation did not change the structure of TiO_2, thus we consider the colored samples to be due to oxygen vacancies on surface of the TiO_2. In order to uncover the influence of the oxygen vacancies on the photoelectric performance, we studied the photoelectric performance of H-TiO_2 with different annealing temperatures in a hydrogen atmosphere. Fig. 2(a) shows the photocurrent–voltage curves of pristine TiO_2 and H-TiO_2 photoelectrodes. The photocurrent density of the pristine TiO_2 nanorod arrays is only 0.13 mA cm^{-2}, but after hydrogenation the photocurrent density increased significantly, and the increment depends on the annealing temperature. From Fig. 2(a), the best photocurrent density is 1.48 mA cm^{-2} after annealing in a hydrogen atmosphere at 300 °C. In our study the photocurrent density of the H-TiO_2 nanorod arrays annealed at 300 °C was 11.4 times higher than that of the pristine TiO_2 nanorod arrays. It confirms that hydrogenation is a simple and

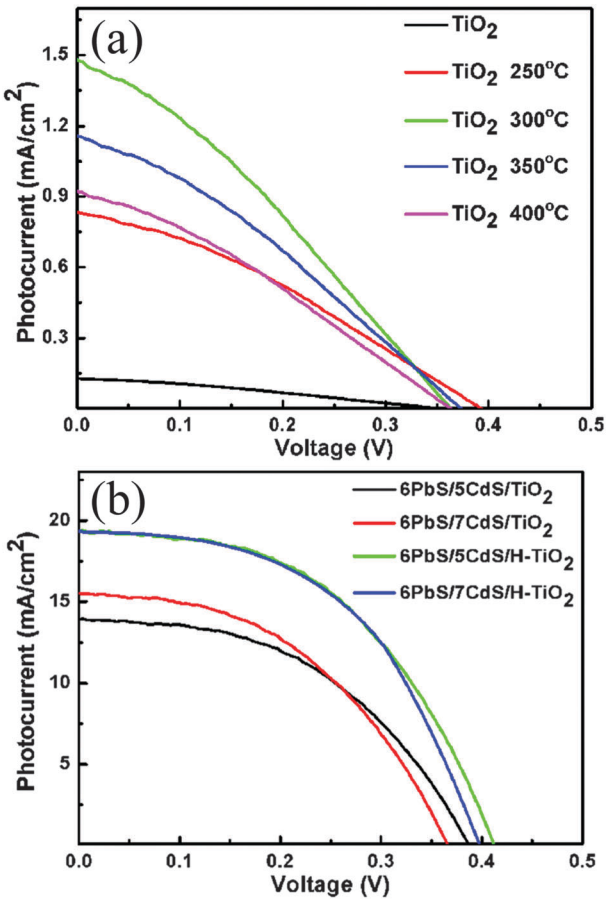

Fig. 2 Photocurrent–voltage curves of photoelectrodes. (a) Pristine TiO_2 nanorod arrays and H-TiO_2 nanorod arrays annealed at different temperatures; (b) multiple semiconductor co-sensitized TiO_2/H-TiO_2 nanorod array solar cells with 3 cycles of ZnS coating.

effective method for enhancing the photoelectric performance of TiO_2 nanorod arrays. Fig. 2(b) and Table S1 (ESI†) show the photocurrent–voltage curves and photoelectric parameters (the short-circuit current density (J_{sc}), open-circuit potential (V_{oc}), fill factor (FF), and total energy conversion efficiency (η)) of PbS/CdS co-sensitized TiO_2 and H-TiO_2 working as photoelectrodes. In Table S1 (ESI†), the best J_{sc}, V_{oc}, FF, and η properties of TiO_2 QDSSCs were 15.52 mA cm^{-2}, 0.37 V, 46.07% and 2.65%, respectively. The highest properties of H-TiO_2 QDSSCs were 19.34 mA cm^{-2}, 0.44 V, 49.05%, and 3.98%, respectively. These results demonstrate that the energy conversion efficiency of H-TiO_2 increased sharply when co-sensitized with PbS/CdS.

To further understand the influence of hydrogenation on photoelectric performance, the TiO_2 nanorod arrays were analyzed with X-ray Photoelectron Spectroscopy (XPS) before and after hydrogenation to determine the chemical states and understand the oxygen vacancies in TiO_2 films. The XPS results are shown in Fig. 3. In the Ti 2p core level spectral pattern (Fig. 3(a)), the binding energies of 458.61 eV (Ti 2p3/2) and 464.28 eV (2p1/2) are assigned to the Ti 2p doublet arising from TiO_2, and are consistent with titanium in +4 state.[10] After hydrogenation, the binding energies of the Ti 2p states are

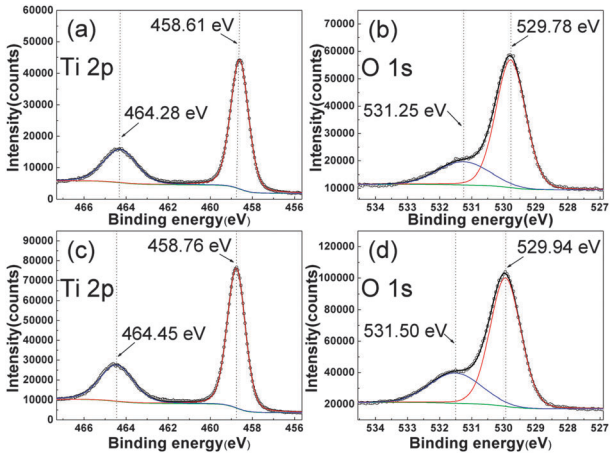

Fig. 3 XPS results of TiO_2 before and after hydrogenation, (a) and (b) are the TiO_2 before hydrogenation; (c) and (d) are the TiO_2 after hydrogenation at 300 °C which has the best photoelectric performance results.

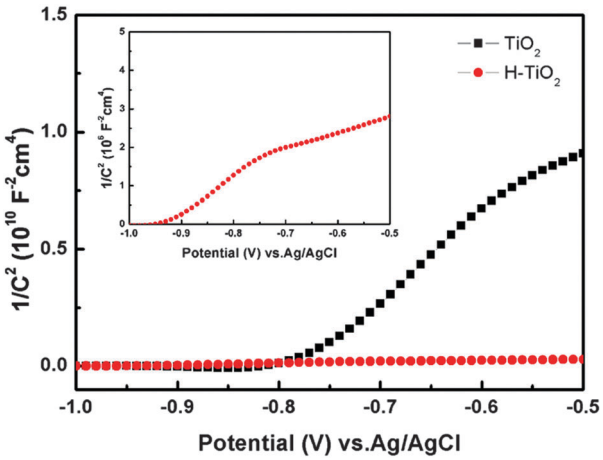

Fig. 4 Mott–Schottky plots collected at a frequency of 5 kHz for the pristine TiO_2 and H-TiO_2 nanorod arrays annealed at 300 °C. Inset is the magnified plot of H-TiO_2.

only about 0.15 eV higher than normal titanium in TiO_2, with no significant changes found. The O 1s spectra obtained from XPS analysis are shown in Fig. 3(b) and (d). Two kinds of state are apparent in the O 1s XPS results, the lower binding energy of 529.78 eV and higher binding energy of 531.25 eV are in accordance with Ti–O bonds and O–H bonds respectively.[11] This demonstrates that the surface of the TiO_2 is hydroxylated both before and after hydrogenation. It is generally known that the surface of TiO_2 is usually covered with a certain amount of titanol (Ti–OH) groups which are dissociated from absorbing water in air.[12] However hydrogenation increases the hydroxy content of TiO_2. The hydroxy content is only 22% of the content of total oxygen before hydrogenation, but increases to 27% after hydrogenation. The increasing hydroxy content indicates that hydrogenation generates the oxygen vacancies on the surface of TiO_2.[13] This is consistent with the experimental results of Simonsen *et al.*[14] Water is adsorbed easily on the surface of TiO_2 and occupies the oxygen vacancies caused by hydrogenation. Thus the hydroxy content increases after hydrogenation due to generation of more oxygen vacancies on the surface of the TiO_2.

According to the diffuse reflectance absorption spectra and $(\alpha h\nu)^2$-photon energy curves (Fig. S3(a) and (b), ESI†), the oxygen vacancies in the TiO_2 enhanced the visible light and near-infrared light absorption, and even narrowed the band gap of the semiconductor.[13] Hence enhancement of the photoelectric performance after hydrogenation can be attributed to the oxygen vacancies on the surface of the TiO_2.

Introducing oxygen vacancies on the surface of TiO_2 actually improves its electrical conduction properties. To further understand the electrical conduction properties, we conducted electrochemical impedance measurements on the pristine TiO_2 and H-TiO_2 nanorod arrays annealed at 300 °C at a frequency of 5 kHz, to investigate the influence of hydrogen treatment on the electronic properties of TiO_2. The TiO_2 and H-TiO_2 nanorod arrays show positive slopes in Mott–Schottky plots, as expected for an n-type semiconductor (Fig. 4). Importantly, the H-TiO_2 has a smaller slope in a Mott–Schottky plot compared to the pristine TiO_2, suggesting an increase of donor densities. Carrier densities of these nanorod arrays were calculated from the slopes of the Mott–Schottky plots using the equation[15]

$$N_d = (2/e_0\varepsilon\varepsilon_0)[d(1/C^2)/dV]^{-1}$$

where e_0 is the electron charge, ε is the dielectric constant of TiO_2 (ε = 170),[16] ε_0 is the permittivity of the vacuum, C is the differential capacity, N_d is the donor density, and V is the applied bias at the electrode. The calculated electron densities of the pristine TiO_2 and H-TiO_2 were 2.112×10^{19} and 8.859×10^{22} cm^{-3}, respectively. Although the Mott–Schottky plots are derived from a flat electrode model and may have errors in determining the absolute value of donor density, hydrogenation leads to a significant enhancement of carrier density in TiO_2, which is evident through a qualitative comparison of the slopes of the Mott–Schottky plots. The enhanced donor density is due to the increased oxygen vacancies. The increased donor density improves the charge transport in TiO_2, as well as electron transfer at the interface between the semiconductor and the FTO substrate. The enhanced electron density is one of the major reasons for the photoelectric performance enhancement. So the high photoelectric performance of H-TiO_2 is due to extending the visible absorption, narrowing the band gap, and enhancing the electron density.

In order to further increase the photoelectric performance, H-TiO_2 was sensitized with QDs (CdS/PbS). The high photoelectric performance of the H-TiO_2 QDSSCs was mentioned above. Because the H-TiO_2 nanorod array QDSSCs were not fully covered by the QDs (Fig. S1(c), ESI†), visible light can be captured by both the QDs and H-TiO_2. So, for the H-TiO_2 QDSSCs, not only the QDs, but also the H-TiO_2 can capture light and extend the visible light absorption compared with the pristine TiO_2 QDSSCs (Fig. S3(c), ESI†). The photoelectric performance of our H-TiO_2 QDSSCs can be considered as the total of the efficiencies of the QDs and the TiO_2. So, H-TiO_2

QDSSCs are an efficient way to improve photoelectric performance.

In summary, this report demonstrates that using hydrogenated TiO_2 nanorod arrays as photoanodes to fabricate PbS/CdS QDSSCs is an effective method to enhance photoelectric performance. The higher efficiency can be attributed to oxygen vacancies on the surface of the TiO_2 caused by hydrogenation. With these results, we demonstrated that hydrogenation is a conceptually different approach to enhance the energy conversion efficiency and to narrow the bandgap by introducing oxygen vacancies on the surface of TiO_2 nanorod array films.

This work was financially supported by the Science and Technology Development Program of Jilin Province (20110417) and the National Natural Science Foundation of China (No. 51272086).

Notes and references

1 T. Bak, J. Nowotny, M. Rekas and C. C. Sorrell, *Int. J. Hydrogen Energy*, 2002, **27**, 991.
2 S. Liu, E. Y. Guo and L. W. Yin, *J. Mater. Chem.*, 2012, **22**, 5031; B. Liu, H. M. Chen, C. Liu, S. C. Andrews, C. Hahn and P. D. Yang, *J. Am. Chem. Soc.*, 2013, **135**, 9995; X. B. Chen and C. Burda, *J. Am. Chem. Soc.*, 2008, **130**, 5018; T. O. He, X. L. Guo, K. Zhang, Y. M. Feng and X. D. Wang, *RSC Adv.*, 2014, **4**, 5880; J. C. Yu, J. G. Yu, W. K. Ho, Z. T. Jiang and L. Z. Zhang, *Chem. Mater.*, 2002, **14**, 3808; S. U. M. Khan, M. Al-Shahry and B. I. J. William, *Science*, 2002, **297**, 2243; R. Asahi, T. Morikawa, T. Ohwaki, K. Aoki and Y. Taga, *Science*, 2001, **293**, 269.
3 S. Tominaka, *Inorg. Chem.*, 2012, **51**, 10136.
4 S. H. Hsu, S. F. Hung and S. H. Chien, *J. Power Sources*, 2013, **233**, 236; L. Li, X. C. Yang, J. J. Gao, H. N. Tian, J. Z. Zhao, A. Hagfeldt and L. C. Sun, *J. Am. Chem. Soc.*, 2011, **133**, 8458; P. K. Santra and P. V. Kamat, *J. Am. Chem. Soc.*, 2012, **134**, 2508.
5 H. Huang, L. Pan, C. K. Lim, H. Gong, J. Guo, M. S. Tse and O. K. Tan, *Small*, 2013, **9**, 3153; H. J. Lee, M. K. Wang, P. Chen, D. R. Gamelin, S. M. Zakeeruddin, M. Grätzel and M. K. Nazeeruddin, *Nano Lett.*, 2009, **9**, 4221.
6 H. J. Lee, P. Chen, S. J. Moon, F. Sauvage, K. Sivula, T. Bessho, D. R. Gamelin, P. Comte, S. M. Zakeeruddin, S. I. Seok, M. Grätzel and M. K. Nazeeruddin, *Langmuir*, 2009, **25**, 7602; L. Etgar, T. Moehl, S. Gabriel, S. G. Hickey, A. Eychmüller and M. Grätzel, *ACS Nano*, 2012, **6**, 3092.
7 Z. K. Zheng, B. B. Huang, J. B. Lu, Z. Y. Wang, X. Y. Qin, X. Y. Zhang, Y. Dai and M. H. Whangbo, *Chem. Commun.*, 2012, **48**, 5733; G. M. Wang, H. Y. Wang, Y. C. Ling, Y. C. Tang, X. Y. Yang, R. C. Fitzmorris, C. C. Wang, J. Z. Zhang and Y. Li, *Nano Lett.*, 2011, **11**, 3026; Y. H. Hu, *Angew. Chem., Int. Ed.*, 2012, **51**, 12410; T. Leshuk, R. Parviz, P. Everett, H. Krishnakumar, R. A. Varin and F. Gu, *ACS Appl. Mater. Interfaces*, 2013, **5**, 1892; S. S. Zhang, S. Q. Zhang, B. Y. Peng, H. J. Wang, H. Yu, H. H. Wang and F. Peng, *Electrochem. Commun.*, 2012, **40**, 24; X. Chen, Y. Song, L. F. Lu, C. W. Cheng, D. F. Liu, X. H. Fang, X. Y. Chen, X. F. Zhu and D. D. Li, *Nanoscale Res. Lett.*, 2013, **8**, 391; W. Wang, Y. R. Ni, C. H. Lu and Z. Z. Xu, *RSC Adv.*, 2012, **2**, 8286; J. Y. Dong, J. Han, Y. S. Liu, A. Nakajima, S. Matsushita, S. H. Wei and W. Gao, *ACS Appl. Mater. Interfaces*, 2014, **6**, 1385.
8 B. Liu and E. S. Aydil, *J. Am. Chem. Soc.*, 2009, **131**, 3985.
9 X. B. Chen, L. Liu, Z. Liu, M. A. Marcus, W. C. Wang, N. A. Oyler, M. E. Grass, B. H. Mao, P. A. Glans, P. Y. Yu, J. H. Gao and S. S. Mao, *Sci. Rep.*, 2013, **3**, 1510.
10 T. Leshuk, R. Parviz, P. Everett, H. Krishnakumar, R. A. Varin and F. Gu, *ACS Appl. Mater. Interfaces*, 2013, **5**, 1892; H. M. Li, Y. S. Zeng, T. C. Huang and M. Liu, *J. Nanopart. Res.*, 2012, **14**, 1030; J. F. Moulder, W. F. Stickle, P. E. Sobol and K. D. Bomben, *Handbook of X-ray Photoelectron Spectroscopy*, Physical Electronics Inc., 1996.
11 A. O. T. Patrocínio, E. B. Paniago, R. M. Paniago and N. Y. M. Iha, *Appl. Surf. Sci.*, 2008, **254**, 1874; R. Sanjinés, H. Tang, H. Berger, F. Gozzo, G. Margaritondo and F. Lévy, *J. Appl. Phys.*, 1994, **75**, 2945; B. Erdem, R. A. Hunsicker, G. W. Simmons, E. D. Sudol, V. L. Dimonie and M. S. El-Aasser, *Langmuir*, 2001, **17**, 2664; G. Iucci, M. Dettin, C. Battocchio, R. Gambaretto, C. D. Bello and G. Polzonetti, *Mater. Sci. Eng., C*, 2007, **27**, 1201; N. Ohtsu, N. Masahashi, Y. Mizukoshi and K. Wagatsuma, *Langmuir*, 2009, **25**, 11586.
12 D. S. Warren and A. J. McQuillan, *J. Phys. Chem. B*, 2004, **108**, 19373.
13 A. Naldoni, M. Allieta, S. Santangelo, M. Marelli, F. Fabbri, S. Cappelli, C. L. Bianchi, R. Psaro and V. D. Santo, *J. Am. Chem. Soc.*, 2012, **134**, 7600; X. B. Chen, L. Liu, P. Y. Yu and S. S. Mao, *Science*, 2011, **331**, 746; L. Zeng, W. L. Song, M. H. Li, D. W. Zeng and C. S. Xie, *Appl. Catal., B*, 2014, **147**, 490; C. K. Zhang, H. M. Yu, Y. K. Li, Y. Gao, Y. Zhao, W. Song, Z. G. Shao and B. L. Yi, *ChemSusChem*, 2013, **6**, 659; Z. F. Zheng, J. Teo, X. Chen, H. W. Liu, Y. Yuan, E. R. Waclawik, Z. Y. Zhong and H. Y. Zhu, *Chem. – Eur. J.*, 2010, **16**, 1202; X. H. Wei, R. L. Zhou, B. Balamurugan, R. Skomski, X. C. Zeng and D. J. Sellmyer, *Nanoscale*, 2012, **4**, 7704.
14 M. E. Simonsen, Z. S. Li and E. G. Søgaard, *Appl. Surf. Sci.*, 2009, **255**, 8054.
15 K. Darowicki, S. Krakowiak and P. Ślepski, *Electrochim. Acta*, 2006, **51**, 2204.
16 R. A. Parker, *Phys. Rev.*, 1961, **124**, 1719.

